Zinc oxide-hydroxyapatite nanocomposite photocatalysts for the degradation of ciprofloxacin and ofloxacin antibiotics

C. El El Bekkali, H. Bouyarmane, M. El Karbane, S Masse, A. Saoiabi, T. Coradin, A. Laghzizil

Zinc oxide-hydroxyapatite nanocomposite photocatalysts for the degradation of ciprofloxacin and ofloxacin antibiotics

C. El Bekkali,[a] H. Bouyarmane,[a] M. El Karbane,[b] S. Masse,[c] A. Saoiabi,[a] T. Coradin,[c,*] A. Laghzizil[a,*]

[a]*Laboratoire de Chimie Appliquée des Matériaux, Université Mohammed V, Faculté des Sciences BP.1014 Rabat, Morocco*

[b]*Laboratoire National de Contrôle des Médicaments, Rabat, Morocco*

[c]*Sorbonne Universités, UPMC Univ Paris 06, CNRS, Collège de France, UMR 7574, Laboratoire de Chimie de la Matière Condensée de Paris, F-75005 Paris, France*

*corresponding authors

thibaud.coradin@upmc.fr (T. Coradin); laghzizi@fsr.ac.ma (A. Laghzizil)

Abstract

Zinc oxide-hydroxyapatite nanocomposites were prepared from a natural phosphate ore *via* a solvent-free method and evaluated for the photodegradation of two antibiotics in solution. The *in situ* growth of ZnO followed by thermal treatment allowed for the formation of photocatalytic nanocrystals homogeneously dispersed in the apatite phase. Nanocomposites exhibited higher rates of sorption of ofloxacin and ciprofloxacin compared to the individual phases. At high ZnO loadings, photodegradation performances of the nanocomposites under UV irradiation were equivalent or greater than that of the photocatalytic particles alone, depending on the considered antibiotic. This dependency reflects distinct degradation pathways that were attributed to different affinities of the antibiotics for the nanocomposite particles. Because of its simplicity and versatility, the here-described approach appears very promising for the development of multifunctional platforms for water remediation.

1. Introduction

Pharmaceutical pollutants represent major contaminants for the water resources whose sanitary and environmental impacts are now fully taken into account and estimated [1,2]. They form a wide class of molecules having variable physical and chemical properties, making them particularly complex to eliminate from wastewaters [3,4]. For instance, the majority of pharmaceuticals are relatively hydrophobic and therefore less effectively removed by simple sorption processes [5,6]. Moreover, due to their intrinsic biological activity, their partial or complete degradation prior to discharge is highly recommended [2]. With this purpose, ozonation and other advanced oxidation technologies have been described [7,8], among which photodegradation appears particularly promising [9]. This technology relies on the use of a photocatalytic material, in most cases a nanoscale semiconductor, able to generate highly oxidative species under light excitation [10]. While titanium dioxide remains the most popular photocatalyst used for pharmaceuticals photodegradation [11], zinc oxide has also shown interesting potentialities in this field [12,13].

The benefits of associating nanoscale photocatalysts with a complementary phase within composite structures have been demonstrated at several occasions [14]. In the case of ZnO-based nanocomposites, it can allow for a pre-concentration of the organic molecules at the vicinity of the photocatalysts, favor the dispersion of the photoactive phase and therefore increase the available reactive surface, permit shaping and recovery of the photoactive material, enhance intrinsic photocatalytic properties and lead to the design of multifunctional materials exhibiting magnetic properties or being able to degrade organics and retain toxic metals [15-20].

Among sorbing phases that may be advantageously associated with ZnO, hydroxyapatite ($Ca_{10}(PO_4)_6(OH)_2$) appears particularly interesting due to its high capacity for metal ions retention and good sorption properties towards certain organic pollutants, including antibiotics [21-26]. The

co-precipitation of hydroxyapatite-based nanocomposites with other inorganic phases, such as ZrO$_2$, Fe$_3$O$_4$ or TiO$_2$, for remediation purpose has already been described [27-29]. In particular, Ti-doped hydroxyapatites have shown very promising properties as photocatalysts [30-33]. Elaborating on these results, we have prepared here hydroxyapatite-ZnO nanocomposites and evaluated their photodegradation efficiency towards two antibiotics belonging to the fluoroquinone family, ciprofloxacin and ofloxacin. In addition to their widespread use, these pharmaceuticals were selected for their previously-reported good affinity for hydroxyapatite surfaces [26]. Other catalysts have been used for the photodegradation of ciprofloxacin such as TiO$_2$-montmorillonite [34], iron [35] and ZnWO$_4$-CdS [36]. In addition, the photocatalytic degradation of ofloxacin was studied on Bi$_2$O$_3$/TiO$_2$ [37]. We show that a purely aqueous synthetic route combining natural phosphate ore and a zinc salt leads to nanosized powders where ZnO photocatalysts are homogeneously associated with the hydroxyapatite particles. We could evidence that the nanocomposites exhibit faster rates of antibiotics sorption compared to both individual phases and, for the highest zinc oxide loadings, similar or faster photodegradation rates than pure ZnO. Our data show that the two antibiotics, although being of similar chemical structure, undergo distinct degradation pathways, that are discussed in terms of surface affinity and diffusion issues.

2. Experimental

2.1. Preparation and characterization of the HAp-ZnO nanocomposites (wZnHAp)

The pure hydroxyapatite powder (HAp) was prepared by a dissolution/reprecipitation method from a natural phosphate ore coming from the Bengurir region (Morocco) as previously described [38]. The dissolution of the ore was carried out by introducing 30 g of the collected raw material in a 2

L reactor containing 500 mL of deionized water acidified to pH 2 by addition of 20 mL of concentrated HNO$_3$ acid (65%), under continuous stirring for 3 hours at room temperature. After filtration, the recovered solution containing calcium and phosphate ions was brought to pH 10 by addition of a concentrated ammonia solution (25 %). The resulting precipitate was aged for 24 h, filtered and washed three times with deionized water with intermediate ultrasound irradiation steps to optimize grain dispersion. Finally, the powder was dried in an oven at 100 °C for 24 h and, when noted, heated to 500°C for 3 h.

Among methods available for zinc oxide synthesis [39], the precipitation route through alkalinization of an acidic solution of zinc nitrate dihydrate Zn(NO$_3$)$_2$.2H$_2$O by ammonium hydroxide addition was selected since it fully parallels the conditions of synthesis of HAp. For the preparation of the nanocomposites, the zinc precursor was added to 200 mL of the calcium and phosphate-containing solution originating from ore dissolution and a concentrated solution of NH$_4$OH (25%) was added up to pH = 10 under continuous stirring at room temperature. The amount of added precursor was varied to obtain a theoretical final ZnO:HAp weight ratio $w = 5$, 10, 25 and 40 % and the resulting materials were named wZnHAp. The resulting gelatinous precipitates were aged for 24 h. After dispersion in water under ultrasound irradiation, the precipitates were filtered and washed three times with water with intermediate ultrasound irradiation steps to optimize grain dispersion. Finally, the powders were dried in an oven at 100 °C for 24 h or 500°C for 3 h.

The resulting solids were characterized using X-ray powder diffraction (XRD) (Philips PW131diffractometer, Cu Kα radiation). Nitrogen sorption isotherms were recorded at 77 K using a Micromeretics ASAP 2010 instrument. Specific surface areas (S_{BET}) and porous volume (Vp) were calculated according to the Brunauer-Emmet-Teller (BET) method whereas the average pore

size (Dp) were calculated using the BJH model. Chemical analyses were performed by inductively coupled plasma atomic emission spectroscopy (ICP-AES).

2.2 Adsorption and photodegradation procedures

The kinetics of the sorption of ciprofloxacin (CIP, 1-Cyclopropyl-6-fluoro-1,4-dihydro-4-oxo-7-(1-piperazinyl)-3-quinolinecarboxylic acid) and ofloxacin (OFL, (R,S)-9-Fluoro-2,3-dihydro-3-methyl-10-(4-methyl-1-piperazinyl)-7-oxo-7H-pyrido(1,2,3-de)-1,4-benzoxazine-6-carboxylic acid) antibiotics (**Fig. 1**) on *w*ZnHAp composites were studied using a batch method. Antibiotics aqueous solutions at a 20 mg · mL^{-1} concentration were prepared in deionized water. 100 mL of these solutions was placed in a 500 mL thermostated reactor and 0.2 g of the thermally-treated samples was added at 25°C using a mechanical stirrer (EUROSTAR digital IKA). At different reaction times (t), aliquots of the supernatant solution were taken with a 2 mL propylene syringe equipped with a 0.45 µm filter and the amount of adsorbed antibiotics q_t (mg · g^{-1}) was measured by the difference between the initial and final concentration of the organic molecule in the solution, as determined by High Performance Liquid Chromatography (HPLC) [26].

These kinetics data were fitted with the linear form of the Lagergren pseudo first-order equation (eq. 1)

$$\log(q_{e,1} - q_t) = \log q_{e,1} - \frac{k_1}{2.303}t$$

where $q_{e,1}$ is the amount at equilibrium of adsorbed molecule per gram of sorbent (in mg · g^{-1}) and k_1 is the pseudo-first order rate constant,

and the linear form of the Lagergren pseudo-second-order equations (eq. 2)

$$\frac{1}{\left(q_{e,2} - q_t\right)} = \frac{1}{q_{e,2}} + k_2 t$$

with $q_{e,2}$, the amount at equilibrium of adsorbed molecule per gram of sorbent (in mg $\cdot$ g^{-1}) and k_2 the pseudo-second order rate constant [40]. The Kaleidagraph software used to perform the fitting procedure provided the coefficient of linear determination (R^2).

The photochemical activity of powders heated at 500°C was evaluated under a 125W UV A-B-C (200–600 nm) irradiation. A solid sample (0.2 g) was first dispersed in 100 mL of antibiotic solution (20 mg $\cdot$L^{-1}) and left to react in the dark for 30 min. The solution was then exposed to UV light under magnetic stirring. At each selected time, the suspensions were centrifuged at 4000 rpm for 20 min, and the supernatants were stored in the dark before analysis by HPLC.

3. Results and discussion

3.1. Characterization of the nanocomposite powders

The resulting nanocomposites were characterized by XRD. After drying at 100°C, broad diffraction peaks of the hydroxyapatite structure were identified for the pure HAp sample at $2\theta \approx 26°$ (002 plane), 31° (211), 32° (112) and 34° (200) (JCPDS 09-0432) (**Fig. 2a**). The ZnO sample showed the main diffraction peaks of the zincite structure at *ca*. 32° (100), 34.5° (002), 36.5° (101), 47.5° (102) and 57° (110) (JCPDS 36-1451). Noticeably, these peaks were not evidenced for any of the *w*ZnHAp powders pattern. In contrast, after heating at 500°C, the diffraction peaks of the zincite phase were apparent in the 25ZnHAp and 40ZnHAp nanocomposite materials (**Fig. 2b**). Application of the Scherer formula was difficult in the nanocomposite structures but indicated an average ZnO crystallite size of 20 nm. Noticeably no secondary phase such as zinc phosphates could be evidenced on the diffractograms.

ICP-AES analyses were performed to determine the Ca, P and Zn amounts in the nanocomposites. An increase in the final Zn/Ca ratio with the amount of introduced of Zn nitrate was observed (**Table 1**). However, except for the 40ZnHAp phase, the experimental value was always larger than the expected (theoretical) value. This would suggest that part of the calcium ions have not reacted to form the hydroxyapatite phase. Since no other phases than HAp et ZnO were evidenced by XRD, the most likely explanation is that a fraction of the Zn^{2+} ions have substituted Ca^{2+} in the apatite structure with unreacted calcium ions have remaining in solution and withdrawn during washing step. In favor of this hypothesis is the observation that the Ca/P ratio decreases with the increasing Zn content. This could also contribute to the absence of visible ZnO diffraction peaks in the 5ZnHAp sample even after calcination at 500°C.

The specific surface area of the powders was calculated from N_2 sorption measurements (**Fig. 3** for dried powders) and application of the BET method. After drying at 100°C, all *w*ZnHAp nanocomposites exhibit close S_{BET} values in the 250-270 $m^2 \cdot g^{-1}$ range, that are higher than that of pure HAp (165 $m^2 \cdot g^{-1}$) and one order of magnitude larger than for ZnO alone (**Table 1**). This strongly suggests that both types of particles are more evenly dispersed (*i.e.* less aggregated) within the nanocomposite powder. Porous volumes of the different powders follow the same trend with *Vp* in the 0.5-0.6 $cm^3 \cdot g^{-1}$ for nanocomposites compared to 0.3 $cm^3 \cdot g^{-1}$ for HAp and 0.03 for ZnO. Average pore size *Dp* were 11-12 nm for *w*ZnHAp, slightly larger (14 nm) for HAp and significantly smaller (4 nm) for ZnO. After thermal treatment at 500°C, all S_{BET} and *Vp* values significantly decreased. Again, the nanocomposite powders showed larger S_{BET} and *Vp* values than HAp and ZnO. Dp values were slightly smaller for all samples except for ZnO where an increase up to 8 nm was measured.

TEM imaging of the dried powders of nanocomposites show aggregates of well-defined hydroxyapatite rod-like particles *ca*. 30-50 nm in length, some of them incorporating electron dense nanoparticles 5- 20 nm in size (**Fig. 4**). These nanoparticles are clearly more abundant in the 40ZnHAp sample compared to the 25ZnHAp powder, suggesting that they correspond to a Zn-rich phase. After heating at 500°C, coalescence of the hydroxyapatite particles is observed, in agreement with the observed decrease in S_{BET} values, and dense nanoparticles appear to have grown in size. Based on XRD data, these can therefore be attributed to ZnO nanocrystals. Noticeably, when the pure ZnO powders were imaged, dense crystals with sizes of 50 nm or larger are observed, with no clear variation between the dried and heated sample. This suggests that the hydroxyapatite network limits the growth of the ZnO nanoparticles within the composite powder.

3.2. Antibiotics adsorption experiments

Since a higher photocatalytic efficiency was expected for crystalline ZnO particles, the following studies were performed using *w*ZnHAp powders heated at 500°C. Kinetics of sorption of CIP and OFL were studied at fixed antibiotics and sorbent amount in the dark. The time to reach equilibrium was longer for CIP compared to OFL and it was adsorbed in similar or larger amounts (**Fig. 5**). For both antibiotics, ZnO powders showed the lowest sorption at equilibrium. Among HAp-containing powders, the highest sorption was achieved for the lowest ZnO amount (5ZnHAp) and then this parameter decreased with increasing zinc oxide content. Finally, pure HAp showed comparable or slightly lower sorption at equilibrium than 40ZnHAp.

To analyze these results in more details, two models were evaluated for the fitting of the experimental data. In most cases, the first-order model led to low R^2 values whereas values larger than 0.999 could be obtained with the second-order model (**Table 2**). The values for sorption

amount at equilibrium varies from *ca*. 1.6 mg· g^{-1} on ZnO for both antibiotics to *ca*. 6.4 and 5.4

mg· g^{-1} on 5ZnHAp for CIP and OFL, respectively. Only a slight difference in sorbed amount was

found between the two antibiotics for pure HAp. Kinetics rates were markedly higher for OFL

compared to CIP in all situations but especially for Zn-rich phases.

3.3. Antibiotics photodegradation tests

In order to achieve the total removal of the studied pharmaceutical compounds, the

photochemical activity of wZnHAp powders heated at 500°C was evaluated under an UV A-B-C

irradiation. A preliminary adsorption period of 30 min was performed in the dark before exposure

to UV light. For pure apatite HAp, the adsorption step was quickly followed by a plateau with no

clear evidence of photo-induced degradation (**Fig. 6**). For ZnO, full degradation of CIP was

achieved within 20 minutes while it took more than 2 hours to observe the full disappearance of

OFL. When nanocomposites are considered, the 5ZnHAp powders were less efficient than ZnO

alone. In contrast, 25ZnHAp and 40 ZnHAp showed a similar CIP degradation capacity and

improved OFL degradation capacity (full disappearance after 1 hour) compared to ZnO. This

strongly suggests that, within such nanocomposites, the lower fraction of photoactive ZnO phase

is counterbalanced by the higher sorption capacity of the HAp phase, acting as a pre-concentrating

surface.

To follow the photodegradation process, the samples were analyzed by HPLC (**Fig. 7**). For

CIP, the peak corresponding to the antibiotic rapidly vanishes with irradiation time with no

significant new signal being observed. In contrast, for OFL, the degradation first leads to the

presence of a new peak at slightly smaller retention time, whose relative intensity rises with time

at the expense of the OFL signal over the first hour. Beyond this irradiation time, both signals

decrease in intensity whereas other peaks at much shorter retention time become more significant and remain visible after 2 h.

Noticeably, the photodegradation of pharmaceutical tablets containing ciprofloxacin or ofloxacin and several excipients, including titanium dioxide particles, has been studied and showed very similar degradation rates and pathways for both antibiotics [41]. Specifically, a number of degradation products with molecular weights close to that of the starting compounds have been identified, the most abundant resulting from the breakdown of the piperazinyl ring in the *7* or *10* position of the molecular backbone of CIP and OFL, respectively (**Fig. 8**). In parallel, the efficient full photodegradation of CIP in solution into small organic products using γ-Fe$_2$O$_3$@ZnO composites has been reported in the literature [42]. These data illustrate that diffusion processes are likely to be of paramount importance for the extent of the photodegradation process. This is in agreement with the fact that a second order model was found to be more adapted for fitting the kinetics data, indicating that reaction kinetics depend both on antibiotic and sorbent concentration. In this context, HPLC data suggest that the early degradation products of OFL are easily released in solution and can therefore enter in competition with the pristine antibiotic for further adsorption and degradation (**Fig. 8a**). In contrast, the degraded forms of CIP may remain adsorbed on the solid phase, being therefore not detectable by HPLC, and undergo further transformation until full degradation (**Fig. 8b**). The question remains of the observed difference between OFL and CIP. Since these molecules have close molecular weight and main pKa values, such a difference may originate from distinct hydrophobicity, as indicated by their *XlogP3* values (http://pubchem.ncbi.nlm.nih.gov) (**Fig. 1**), with a higher affinity of the most hydrophilic CIP for the hydroxylated inorganic surfaces. Steric effects due to the presence of a six-membered

heterocycle linked to the pyridine in OFL compared to a three-membered cyclopropyl in CIP can also contribute to this difference.

4. Conclusion

We demonstrate that zinc oxide-hydroxyapatite nanocomposites prepared by a solvent-free route are efficient catalysts for the photodegradation of ciprofloxacin and ofloxacin antibiotics in aqueous solutions under UV irradiation. High Zn loadings within the composite structure can even lead to superior activity compared to the oxide phase alone, thanks to the smaller size and better dispersion of the ZnO nanocrystals. However the two molecules undergo distinct degradation pathways that appear related to their affinity for the photocatalyst surface. Extension to other antibiotics belonging to the same fluoroquinolone family should allow to clarify the underlying mechanisms before exploring a wider range of pharmaceuticals. In parallel, due to the simplicity and versatility of the synthetic process, it is now possible to envision the simultaneous incorporation of several photoactive phases, such as TiO_2 or CeO_2, to improve further the photocatalytic efficiency of these materials.

References

[1] T. Heberer, K. Reddersen, A. Mechlinski, From municipal sewage to drinking water: fate and removal of pharmaceutical residues in the aquatic environment in urban areas, Water Sci. Technol. 46 (2002) 81-88.

[2] J. Martin, D. Camacho-Muñoz, J.L. Santos, I. Aparicio, E. Alonso, Occurrence of pharmaceutical compounds in wastewater and sludge from wastewater treatment plants: removal and ecotoxicological impact of wastewater discharges and sludge disposal, J. Hazard. Mater. 15 (2012) 40-47.

[3] A. J. Watkinson, E. J. Murby, S. D. Constanzo, Removal of antibiotics in conventional and advanced wastewater treatment: implications for environmental discharge and wastewater recycling, Water Res. 41 (2007) 4164–4176.

[4] A. Jelic, M. Gros, A. Ginebreda, R. Cespedes-Sánchez, F. Ventura, M. Petrovic, D. Barcelo, Occurrence, partition and removal of pharmaceuticals in sewage water and sludge during wastewater treatment, Water Res. 45 (2011) 1165–1176.

[5] T. X. Bui, H. Choi, Adsorptive removal of selected pharmaceuticals by mesoporous silica SBA-15, J. Hazard. Mater. 168 (2009) 602-608

[6] S. W. Nam, D. J. Choi, S. K. Kim, N. Her, K. D. Zoh, Adsorption characteristics of selected hydrophilic and hydrophobic micropollutants in water using activated carbon, J. Hazard. Mater. 270 (2014) 144–152.

[7] M. M. Huber, S. Canonica, G. Y. Park, U. von Gunten, Oxidation of pharmaceuticals during ozonation and advanced oxidation processes. Environ. Sci. Technol. 37 (2003) 1016–1024.

[8] G. Boczkaj, A. Fernandes, Wastewater treatment by means of advanced oxidation processes at basic pH conditions: A review, Chem. Eng. J. 320 (2017) 608-633

[9] P. A. Reddy, P. V. Reddy, E. Kwon, K. H. Kim, T. Akter, S. Kalagara, Recent advances in photocatalytic treatment of pollutants in aqueous media, Environ. Int. 91(2016) 94-103.

[10] J. Zhao, C. Chen, W. Ma, Photocatalytic degradation of organic pollutants under visible light irradiation, Top. Catal. 35 (2005) 269-278.

[11] U. I. Gaya, A. H. Abdullah, Heterogeneous photocatalytic degradation of organic contaminants over titanium dioxide: A review of fundamentals, progress and problem, J. Photochem. Photobiol. C 9 (2008) 1-12

[12] K. M. Lee, C. W. Lai, K. S. Ngai, J. C. Juan, Recent developments of zinc oxide based photocatalyst in water treatment technology: A review, Water. Res. 88 (2016) 428-448.

[13] N. L. Fincur, J. B. Krstic, F. S. Sibul, D. V. Sojic, V. N. Despotovic, N. D. Banic, J. R. Agbaba, B. F. Abramovic, Removal of alprazolam from aqueous solutions by heterogeneous photocatalysis: Influencing factors, intermediates, and products, Chem. Eng. J. 307 (2017) 1105-1115.

[14] F. Fresno, R. Portela, S. Suarez, J. M. Coronado, Photocatalytic materials: recent achievements and near future trends, J. Mater. Chem. A 2 (2014) 2863-2884

[15] J. Mu, C. Shao, Z. Guo, Z. Zhang, M. Zhang, P. Zhang, B. Chen, Y. Liu, High photocatalytic activity of ZnO-carbon nanofiber heteroarchitectures. ACS Appl. Mater. Interfaces 3 (2011) 590-596

[16] V. Eskizeybek, F, Sari, H. Gülce, A. Avci, Preparation of the new polyaniline/ZnO nanocomposite and its photocatalytic activity for degradation of methylene blue and malachite green dyes under UV and natural sun lights irradiations, Appl. Catal. B 119–120 (2012) 197-206

[17] A. Rajeswari, S. Vismaiya, A. Pius, Preparation, characterization of nano ZnO-blended cellulose acetate-polyurethane membrane for photocatalytic degradation of dyes from water, Chem. Eng. J. 313 (2017) 928-937

[18] T. S. Anirudhan, J. R. Deepa, Nano-zinc oxide incorporated graphene oxide/nanocellulose composite for the adsorption and photocatalytic degradation of ciprofloxacin hydrochloride from aqueous solutions, J. Colloid Interface Sci. 490 (2017) 343-356.

[19] K. S. Ranjith, P. Manivel, R. T. Rajendrakumar, T. Uyar, Multifunctional ZnO nanorod-reduced graphene oxide hybrids nanocomposites for effective water remediation: Effective sunlight driven degradation of organic dyes and rapid heavy metal adsorption, Chem. Eng. J. 325 (2017) 588-600

[20] J. Fenoll, I. Garrido, M. Pastor-Belda, N. Campilo, P. Viñas, M. J. Yañez, N. Vela, S. Navarro. Solar detoxification of water polluted with fungicide residues using ZnO-coated magnetic particles. Chem. Engin. J. 330 (2017) 71-81.

[21] A. Nzihou, P. Sharrock, Role of phosphate in the remediation and reuse of heavy metal polluted wastes and sites, Waste Biomass Valor. 1 (2010) 163-174

[22] X. Cao, L.Q. Ma, D.R. Rhue, C.S. Appel, Mechanisms of lead, copper, and zinc retention by phosphate rock, Environ. Pollut. 131 (2004) 435–444.

[23] A. Dybowska, D.A.C. Manning, M.J. Collins, T. Wess, S. Woodgate, E. Valsami- Jones, An evaluation of the reactivity of synthetic and natural apatites in the presence of aqueous metals, Sci. Total Environ. 407 (2009) 2953–2965

[24] H. Bouyarmane, S. El Asri, A. Rami, C. Roux, M.A. Mahly, A. Saoiabi, T. Coradin, A. Laghzizil, Pyridine and phenol removal using natural and synthetic apatites as low-cost sorbents: influence of porosity and surface interactions, J. Hazard. Mater. 181 (2009) 736–741.

[25] K. Lin, Y. Pan, R. Chen, X. Cheng, X. Xu, Study of the adsorption of phenol from aqueous solution onto apatite nanopowders, J. Hazard. Mater. 161 (2009)231–240.

[26] H. Bouyarmane, I. El Hanbali, M. El Karbane, A. Rami, A. Saoiabi, S. Saoiabi, S. Masse, T. Coradin, A. Laghzizil, Parameters influencing ciprofloxacin, ofloxacin, amoxicillin and sulfamethoxazole retention by natural and converted calcium phosphates, J. Hazard. Mater. 291 (2015) 38-44.

[27] K. Achelhi, S. Masse, G. Laurent, C. Roux, A. Laghzizil, A. Saoiabi, T. Coradin, Ultrasound-assisted synthesis of mesoporous zirconia-hydroxyapatite nanocomposites and their dual surface affinity for $Cr^{3+}/Cr_2O_7^{2-}$ ions, Langmuir 27 (2011) 15176-15184.

[28] H. Yang, S. Masse, M. Rouelle, E. Aubry, Y. Li, C. Roux, Y. Journaux, L. Li, T. Coradin, Magnetically recoverable iron oxide-hydroxyapatite nanocomposites for lead removal, Int. J. Environ. Sci. Technol. 12 (2015) 1173-1182.

[29] H. Bouyarmane, S. Saoiabi, I. El Hanbali, M. El Karbane, A. Rami, S. Masse, A. Laghzizil, T. Coradin, Porous hydroxyapatite-TiO_2 nanocomposites from natural phosphates and their decolorization properties, Eur. Phys. J. Special Topics 224 (2015) 1863-1871.

[30] A. Nakajima, K. Takakuwa, Y. Kameshima, M. Hagiwara, S. Sato, Y. Yamamoto, N. Yoshida, T. Watanabe, K. Okada, Preparation and properties of titania-apatite hybrid films, J. Photochem. Photobiol. A 177 (2006) 94-99.

[31] G. Sheng, L. Qiao, Y. Mou, Preparation of TiO_2/hydroxyapatite composite and its photocatalytic degradation of methyl orange, J. Environ Eng. 137 (2011) 611-616.

[32] K. Kandori, Y. Yamaguchi, M. Wakamura, Photodecomposition of surfactants using Ti(IV)-doped calcium hydroxyapatite particles, Colloid Polym. Sci. 295 (2017) 1079-1087.

[33] C. Piccirillo, P. M. L. Castro, Calcium hydroxyapatite-based photocatalysts for environment remediation: characteristics, performances and future perspectives, J. Environ. Manage. 193 (2017) 79-91.

[34] A.Hassani, A. Khataee, S. Karaca, Photocatalytic degradation of ciprofloxacin by synthesized TiO_2 nanoparticles on montmorillonite: Effect of operation parameters and artificial neural network modeling, J. Mol. Catal. A: Chem. 409 (2015) 149-161

[35] M. Bobu, A.Yediler, I.Siminiceanu, S.Schulte-Hostede Degradation studies of ciprofloxacin on a pillared iron catalyst, Appl. Catal. B: Environ.83 (2008) 15-23

[36] P. Huo, Y. Tang, M. Zhou, J. Li, Z. Ye, C. Ma, L.Yu, Y. Yan, Fabrication of $ZnWO_4$-CdS heterostructure photocatalysts for visible light induced degradation of ciprofloxacin antibiotics, J. Ind. Eng. Chem. 37 (2016) 340-346

[37] S. Sood, S. K. Mehta, A.S.K. Sinha, S.K. Kansal, Bi_2O_3/TiO_2 heterostructures: Synthesis, characterization and their application in solar light mediated photocatalyzed degradation of an antibiotic, ofloxacin, Chem. Engin. J. 290 (2016) 45-52.

[38] S. El Asri, A. Laghzizil, A. Saoiabi, A. Alaoui, K. Al Abassi, R. M'hamdi, T. Coradin, A novel process for the fabrication of nanoporous apatites from Moroccan phosphate rock, Colloid Surf. A 350 (2009) 73-78.

[39] A. Kolodziejczak-Radzimska, T. Jesionowski, Zinc oxide-from synthesis to application: a review, Materials 7 (2014) 2833-2881.

[40] Y.S. Ho, Review of second-order models for adsorption systems, J. Hazard. Mater. 136 (2006) 681-689.

[41] U. Hubicka, P. Zmudzki, P. Talik, B. Zuromska-Witek, J. Krzek, Photodegradation assessment of ciprofloxacin, moxifloxacin, norfloxacin and ofloxacin in the presence of excipients from tablets by UPLC-MS/MS and DSC, Chem. Cent. J. 7 (2013) 133

[42] N. Li, J. Zhang, Y. Tian, J. Zhao, J. Zhang, W. Zuo, Precisely controlled fabrication of magnetic 3D γ-Fe$_2$O$_3$@ZnO core-shell photocatalyst with enhanced activity: Ciprofloxacin degradation and mechanism insight, Chem. Eng. J. 308 (2017) 377-385.

Table 1. Calculated Ca/P and Zn/Ca ratio from ICP measurements, theoretical Zn/Ca ratio, specific surface area (S_{BET}), porous volume (V_p) and average pore size (D_p) from N_2 sorption for powders treated at 100°C and 500°C

	Ca/P	Zn/Ca Exp.	Zn/Ca The.	$S_{BET}100$ (m^2g^{-1})	V_p100 $(cm^3 g^{-1})$	D_p100 (nm)	$S_{BET}500$ (m^2g^{-1})	V_p500 $(cm^3 g^{-1})$	D_p500 (nm)
HAp	1.89	-	-	165	0.32	14	105	0.26	12
5ZnHAp	1.78	0.12	0.06	270	0.62	12	165	0.35	11
10ZnHAp	1.73	0.18	0.12	265	0.58	12	165	0.34	11
25ZnHAp	1.70	0.36	0.30	260	0.60	12	155	0.33	12
40ZnHAp	1.65	0.48	0.48	250	0.50	11	135	0.22	11
ZnO	-	-	-	20	0.03	4	10	0.02	9

Table 2. Kinetic rate constants (k_i) and adsorption capacities ($q_{e,i}$) as obtained by using pseudo-first order and pseudo-second order models for CIP and OFL sorption on heated wZnHAp composites and pure HAp and ZnO. R^2 indicate the correlation coefficients for the linear fits.

		Pseudo first order			Pseudo second order		
		k_1	$q_{e,1}$	R^2	k_2	$q_{e,2}$	R^2
		(min^{-1})	$(mg\ g^{-1})$		$(g\ mg^{-1}min^{-1})$	$(mg\ g^{-1})$	
HAp	CIP	0.099	2.89	0.9495	0.064	4.27	0.9999
	OFL	0.032	2.08	0.8214	0.156	4.13	0.9999
5ZnHAp	CIP	0.047	3.62	0.9790	0.032	6.36	0.9998
	OFL	0.062	5.12	0.8747	0.840	5.39	0.9999
10ZnHAp	CIP	0.056	3.23	0.9627	0.038	5.47	0.9995
	OFL	0.050	2.51	0.9693	0.844	4.78	0.9998
25ZnHAp	CIP	0.140	4.22	0.9844	0.063	4.83	0.9993
	OFL	0.059	2.95	0.8093	1.271	4.56	0.9993
40ZnHAp	CIP	0.073	2.21	0.9224	0.081	4.65	0.9998
	OFL	0.023	1.65	0.9159	1.256	4.13	0.9997
ZnO	CIP	0.046	1.52	0.9933	0.052	1.59	0.9940
	OFL	0.034	1.47	0.9810	1.794	1.61	0.9951

Figure Captions

Figure 1. Chemical structure and selected physico-chemical parameters for ciprofloxacin and ofloxacin

Figure 2. X-Ray diffractograms of the *w*ZnHAp composite powders compared to pure HAp and ZnO (a) dried at 100°C and (b) calcined at 500°C. Z = zincite; H = Hydroxyapatite

Figure 3. N_2 sorption curves of the *w*ZnHAp composite powders compared to pure HAp and ZnO dried at 100°C

Figure 4. TEM images of 25ZnHAp (a,d), 40 ZnHAp (b,e) and ZnO (c,f) dried at 100°C (a-c) or heated at 500°C (d-e). White arrows indicate darker nanoparticles attributed to ZnO.

Figure 5. Kinetics of (a) ciprofloxacin and (b) ofloxacin removal (q_e) by the *w*ZnHAp composite powders heated at 500°C compared to pure HAp and ZnO. Plain lines show the results of data fitting using the pseudo-second order Lagergren model.

Figure 6. Kinetics of (a) ciprofloxacin and (b) ofloxacin removal (q_e) by the *w*ZnHAp composite powders heated at 500°C compared to pure HAp and ZnO during a first 30 min period in the dark following by irradiation using a 125W UV A-B-C lamp.

Figure 7. HPLC analysis of (a) CIP and (b) OFL solutions during the photodegradation test.

Figure 8. Proposed mechanisms of (a) CIP and (b) OFL photodegradation. Chemical structure of main primary photodegradation products was based on the literature [41].
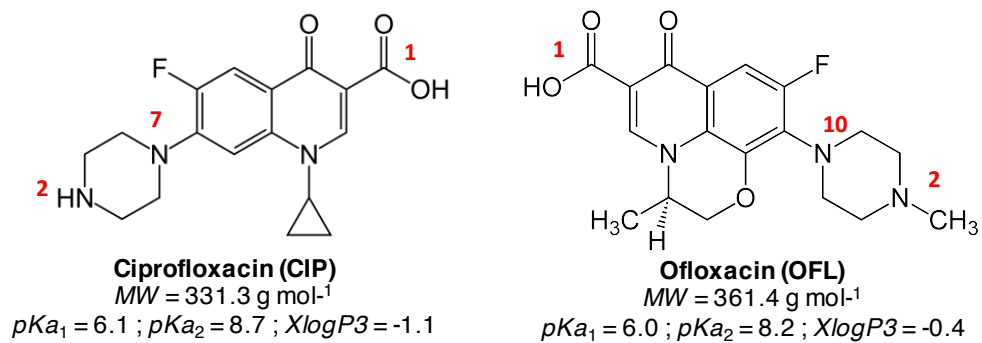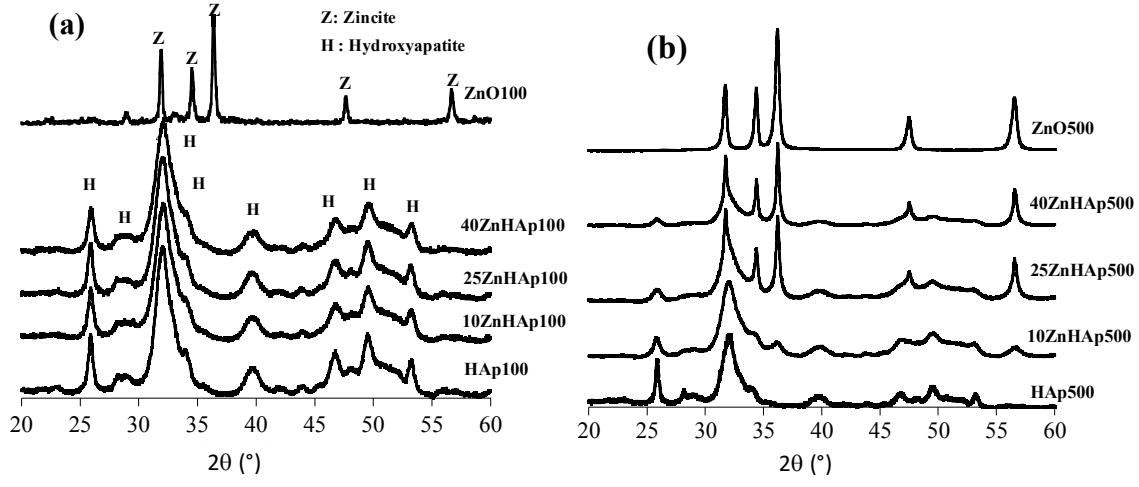
Figure 1.

Ciprofloxacin (CIP)
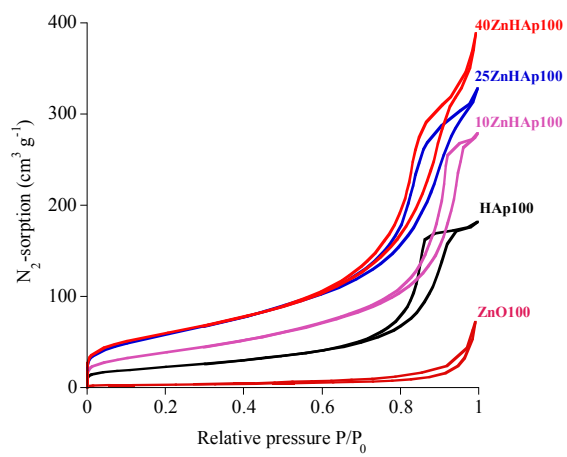$MW = 331.3$ g mol^{-1}
$pKa_1 = 6.1$; $pKa_2 = 8.7$; $XlogP3 = -1.1$

Ofloxacin (OFL)
$MW = 361.4$ g mol^{-1}
$pKa_1 = 6.0$; $pKa_2 = 8.2$; $XlogP3 = -0.4$
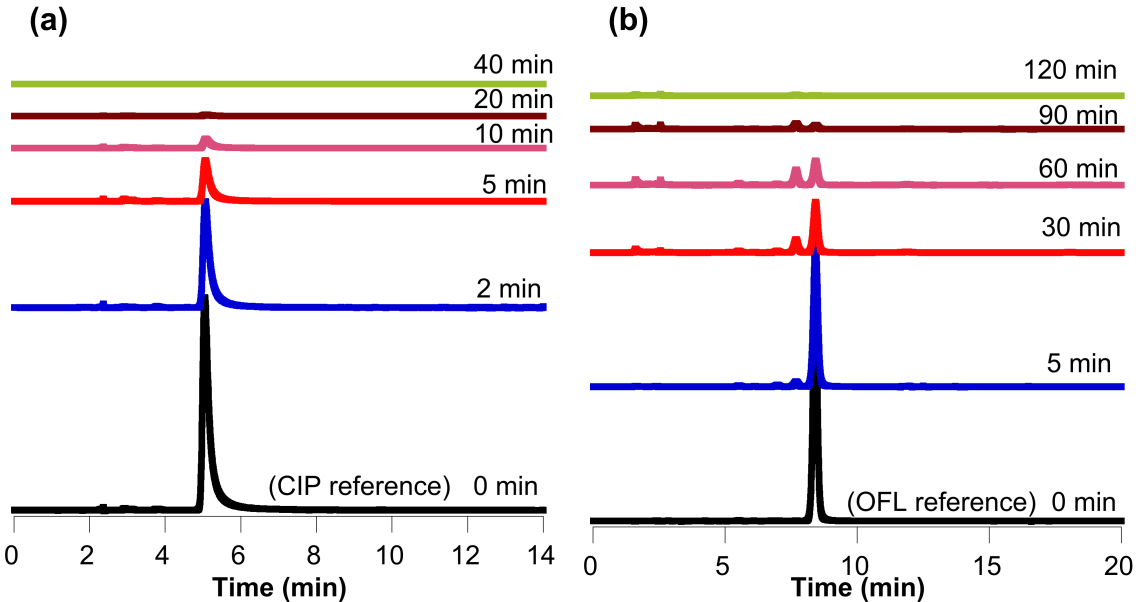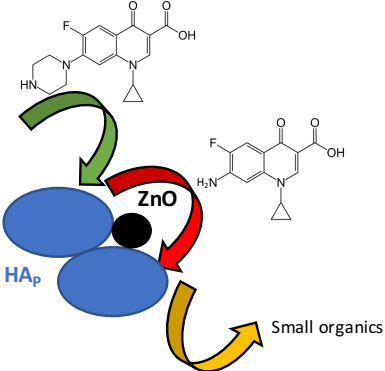
Figure 2.

Figure 3.

Figure 4.
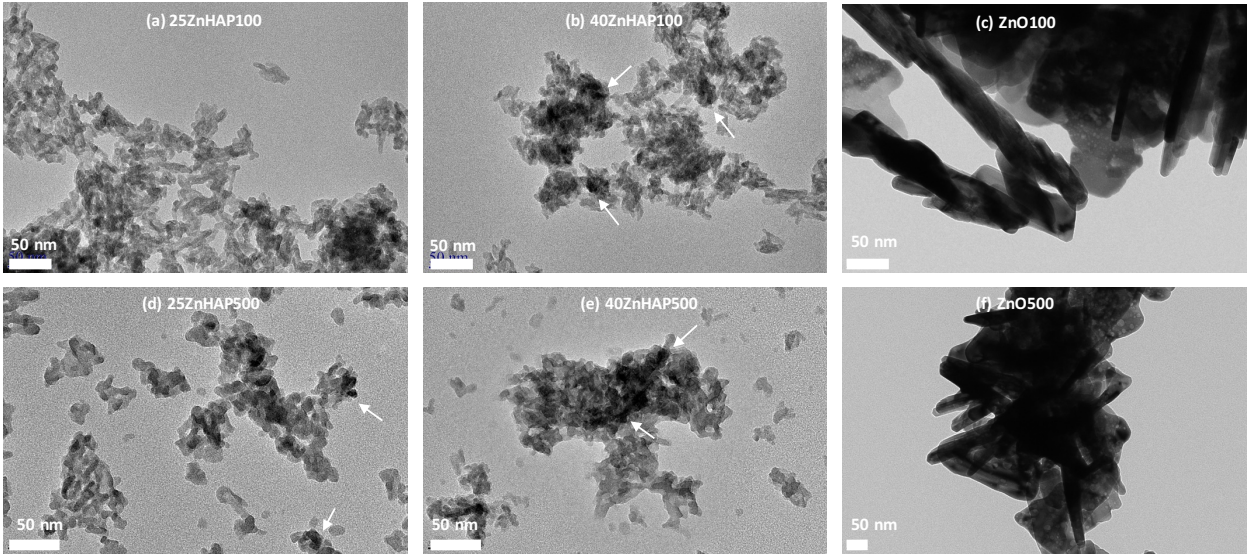
Figure 5.
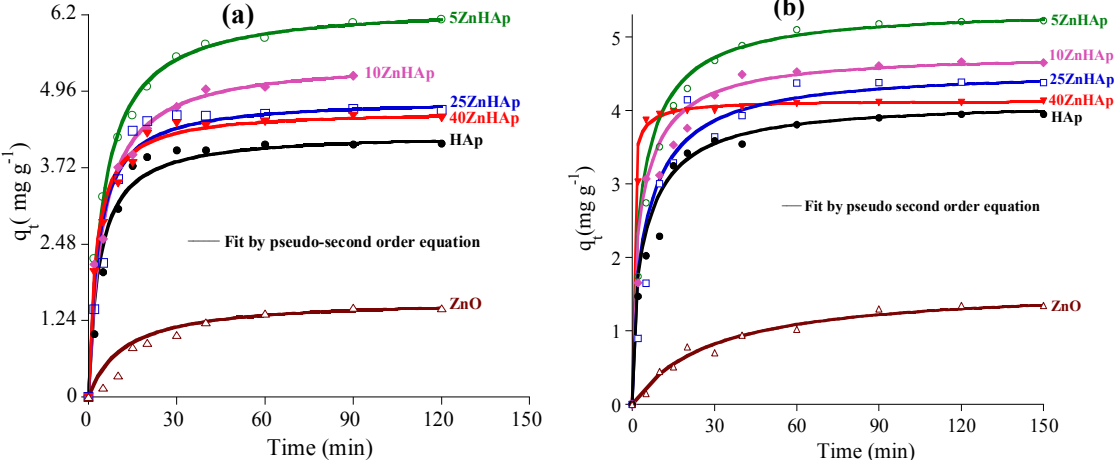
Figure 6.
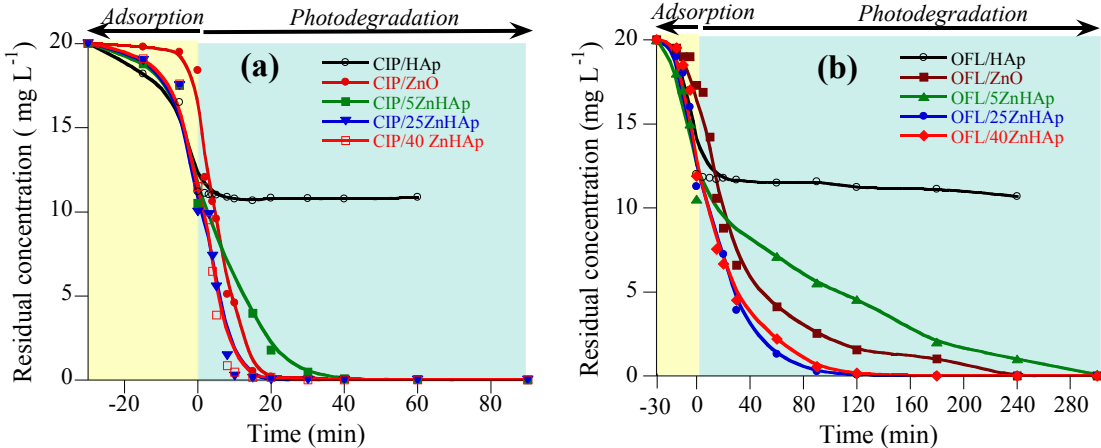
Figure 7.

Figure 8.

(a) CIP

(b) OFL

ZnO

HA_P

Small organics

adsorption   photodegradation   desorption